Electronic Supplementary Material (ESI) for Inorganic Chemistry Frontiers.

Supplementary Information

Fabrication of Cu(I)-Carboxylate Metal-Organic Framework by Reduction of Metal Nodes for Azide-Alkyne "Click" Reaction

Xiaojiao Hou,[a, b] Wenxiu He,[a] Xu Zhai,[a] Bingbing Chen,[a] Yuanlin Fu,[a] Liying Zhang,[a] Junyi Chen*[c] and Yu Fu*[a]

a. Department of Chemistry, College of Sciences, Northeastern University, Shenyang, 110819, P. R. China.

b. Experimental Center, LiaoDong University, Dandong, 118003, P. R. China.

c. Engineering Laboratory of Chemical Resources Utilization in South Xinjiang, College of Chemistry and Chemical Engineering, Tarim University, Xinjiang Uygur Autonomous Region, Alaer, 843300, P. R. China.

*Corresponding authors.

E-mail: fuyu@mail.neu.edu.cn (Yu Fu), sln5xn@163.com (Junyi Chen)

Chemicals

Copper-(II) acetate ($Cu(OAc)_2$), 2,5-dihydroxyterephthalic acid (H_4DOBDC), acetonitrile (MeCN), *N*, *N*-Dimethylformamide (DMF), methanol, ascorbic acid (AA), and hydroquinone (H_2Q) were purchased from Sinopharm Chemical Reagent Co., Ltd. All chemicals were used without further purification.

Characterization

Morphological images of all samples were characterized by field-emission scanning electron microscopy (SEM, Hitachi SU8010) and transmission electron microscope (TEM, FEI Talos F200X). The crystallographic information was obtained by X-ray diffraction (XRD, Panalytical, Empyrean) equipped with a Cu Kα radiation source (λ=0.15406 Å). The organic groups of the samples were characterized by Fourier transform infrared spectroscopy (FT-IR, Bruker VERTEX 70). Thermogravimetric analysis curves were obtained from a TGA thermogravimetric analyzer (PE STA8000) from 25 to 600 °C with a heating rate of 10 °C min^{-1} in air flow. The N_2 adsorption−desorption isotherm was collected using a Surface Area and Porosimetry System (Autosorb-IQ-MP-C). The absorbance of the reducing solution was monitored by UV-vis spectra (Maya2000 Pro). The element content analysis was detected by an inductively coupled plasma spectrometer (ICP, PerkinElmer Avio 500). X-ray photoelectron spectroscopy (XPS) analysis was performed using an X-ray photoelectron spectrometer (Thermo Scientific K-Alpha). GC analysis was performed using a BEIFEN 3420A instrument equipped with a FID (flame ionization detector) and a KB-1701 column (30 m × 0.32 mm × 0.25 μm). ^1H and ^{13}C NMR spectra were measured on a Bruker 600 MHz NMR spectrometer.

X-ray Absorption Spectroscopy Analysis

The extended X-ray absorption fine structure (EXAFS) measurements were carried out on the sample at 5S1 X-ray absorption beamline of Aichi Synchrotron Radiation Center. This beamline adopted a double-bounce channel-cut Si (111) monochromator for mono-beam X-ray absorption spectroscopy. The end-station is equipped with three ionization chambers and seven-elements SDD detector after the sample position for transmission and fluorescence mode X-ray absorption spectroscopy. The photon flux on the sample ranges from 3×10^{10} ~ 4×10^{10} photon/sec for X-ray energy from 5 keV ~ 9 keV in low energy mode. The photon flux on the sample ranges from 1×10^{11} ~ 2.2×10^{10} photon/sec for X-ray energy from 7 keV ~ 18 keV in normal energy mode. The photon flux on the sample ranges from 2.3×10^{10} ~ 5×10^{9} photon/sec for X-ray energy from 17 keV ~ 22 keV in high energy mode.

Synthesis of the metastable CuH_2DOBDC MOF

The 70 mM $Cu(OAc)_2$ solution and the 40 mM 2,5-dihydroxyterephthalic acid (H_4DOBDC) solution were separately prepared using a mixed solvent of DMF and MeCN in a 2:1 volume ratio. Subsequently, 800 μL of the $Cu(OAc)_2$ solution was gradually and dropwise into 4 mL of the H_4DOBDC solution in a glass culture dish while gently shaking. Following evaporation under conditions of room temperature and less than 30% humidity for 24 h, green block crystals were obtained. These crystals were washed with DMF and dried at room temperature.

Reduction of CuH_2DOBDC with different amounts of ascorbic acid

The obtained CuH_2DOBDC (0.1g, 0.2 mmol) was placed in a glass culture dish. In separate vials, we prepared ascorbic acid solutions by dissolving varying amounts of ascorbic acid (0.2, 0.6, 1.0, and 1.4 mmol) in 10 mL of DMF. Once the respective ascorbic acid solution was added to the glass culture dish containing CuH_2DOBDC, it was placed at room temperature for 24 h. Finally, the sample was washed three times with DMF and collected after vacuum freeze-drying.

Reduction of CuH_2DOBDC with different amounts of hydroquinone

The obtained CuH_2DOBDC (0.1g, 0.2 mmol) was placed in a glass culture dish. In separate vials, we prepared hydroquinone solutions by dissolving varying amounts of hydroquinone (1.0, 2.0, 6.0, and 10.0 mmol) in 10 mL of DMF. Once the respective hydroquinone solution was added to the glass culture dish containing CuH_2DOBDC, it was placed at room temperature for 24 h. Finally, the sample was washed three times with DMF and collected after vacuum freeze-drying.

General Procedure for the CuAAC Reaction

A mixture consisting of azides (1 mmol), alkynes (2 mmol), amyl acetate (1 mmol), catalyst (10 mg), and acetonitrile (4 mL) was sealed in a 50 mL sample vial. The resulting mixture was stirred at 80°C. After completion of the reaction, the mixture was centrifuged to recover the catalyst. The recovered catalyst was washed with acetonitrile and methanol, dried, and reused in a subsequent reaction. Product yields were measured by GC, and the products were further confirmed by ^{1}H NMR and ^{13}C NMR spectra on a Bruker 600 MHz spectrometer using $CDCl_3$.

TGA analysis

The residual material was simply CuO under air atmosphere for the TGA test. Both physisorbed water molecules and solvent molecules within the pores cannot be precisely quantified stoichiometrically, whereas the loss of ligands can.[1] Based on FTIR spectroscopy results, it was observed that there is no evidence of DMF participating in the coordination environment of Cu_2H_2DOBDC. Consequently, we propose that the chemical formula of the final products is Cu_xH_2DOBDC (x > 1). Assuming a complete reduction of all Cu(II) in CuH_2DOBDC to Cu(I), the stoichiometric ratio of Cu to H_2DOBDC^{2-} ligand would be 2, in accordance with the principle of valence balance. Therefore, we anticipate a weight loss, relative to this final step, of 50.62% based on the following equation.

$$\frac{M(CuO)}{M(Cu_2H_2DOBDC)} = \frac{160}{324} \times 100\% = 49.38\%$$

The experimental results revealed a relative weight loss of 49.09% (from 93.72% to 44.63% by weight). This experimental value is much closer to the theoretical value (50.62%), thus validating our proposed chemical formula.

EA analysis

The EA results revealed that the content of C in Cu_2H_2DOBDC is 28.6%, thus confirming that the content of the ligand H_4DOBDC is approximately 58.39%. The result is very close to the theoretical content of ligands (60.49%) in the Cu_2H_2DOBDC structure.

The EA results indicate that the N content in Cu_2H_2DOBDC is less than 0.1%.

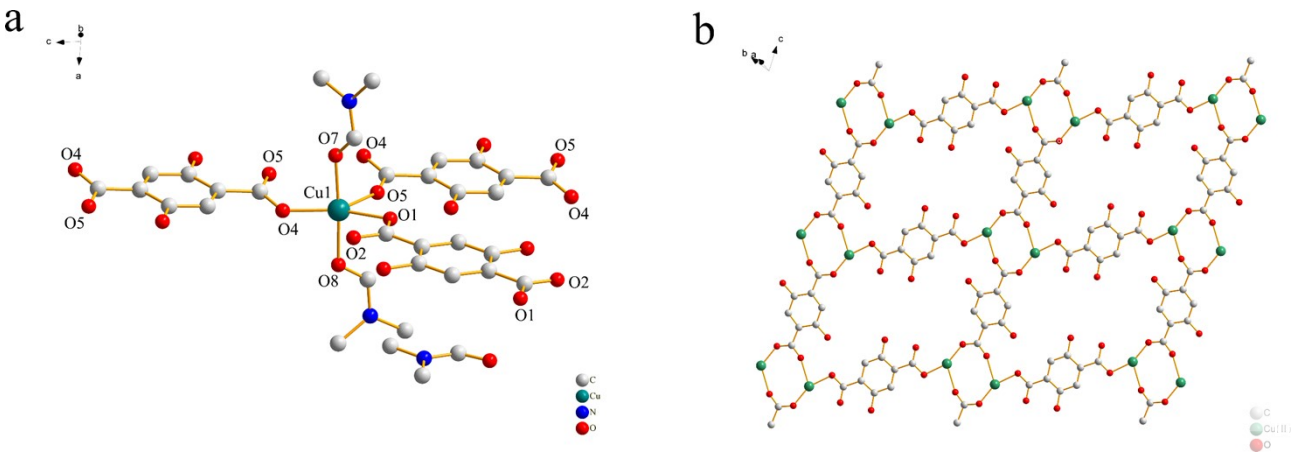

Figure S1. Crystal structure of CuH_2DOBDC. (a) The fundamental unit of CuH_2DOBDC. (b) The 2D layer structure of CuH_2DOBDC. All hydrogen atoms and DMF molecules are omitted for clarity.

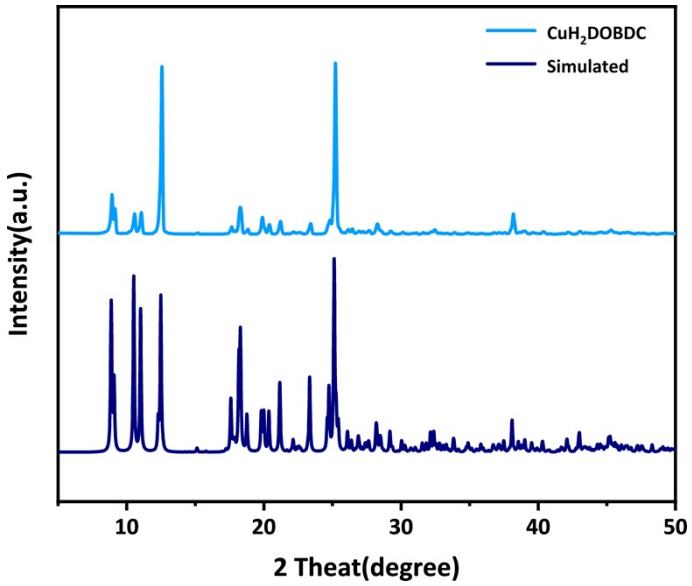

Figure S2. XRD patterns of the prepared metastable CuH_2DOBDC MOF and simulated CuH_2DOBDC MOF.

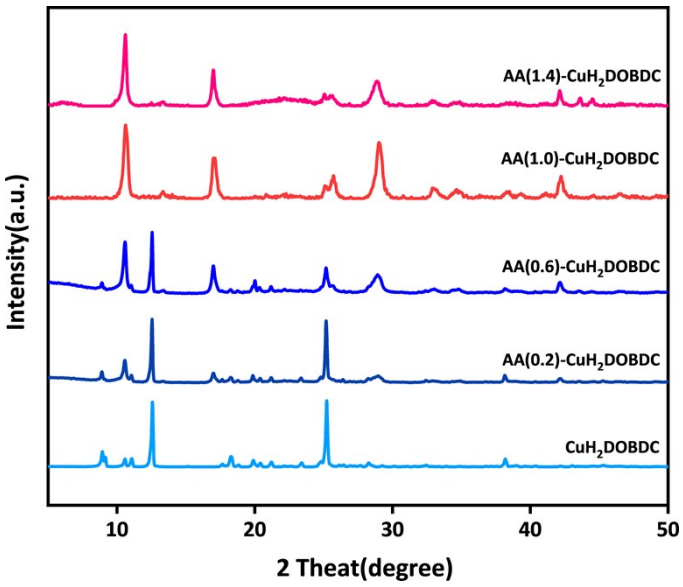

Figure S3. XRD patterns of samples synthesized by reduction of CuH_2DOBDC with different amounts of ascorbic acid.

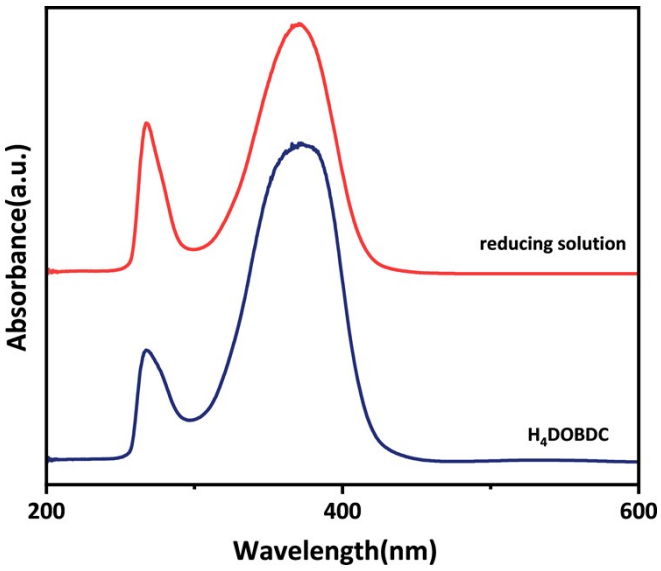

Figure S4. The UV-Vis absorption spectrum of CuH_2DOBDC in an ascorbic acid reducing solution after 24 h.

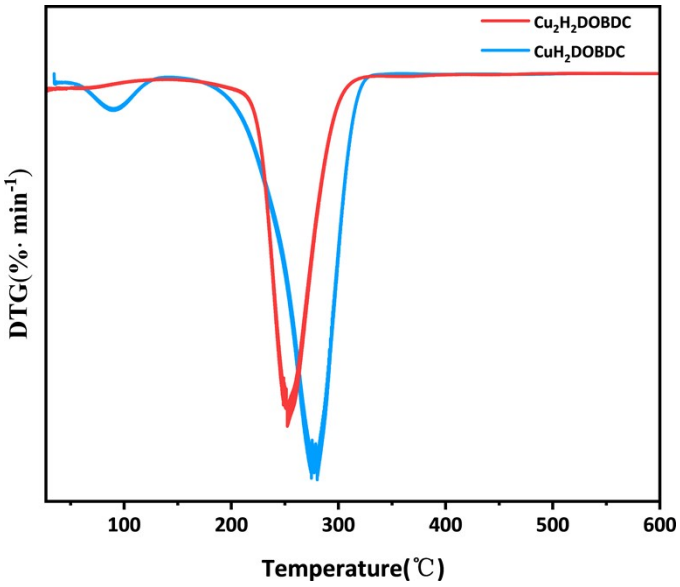

Figure S5. DTG curves of CuH_2DOBDC and Cu_2H_2DOBDC.

a

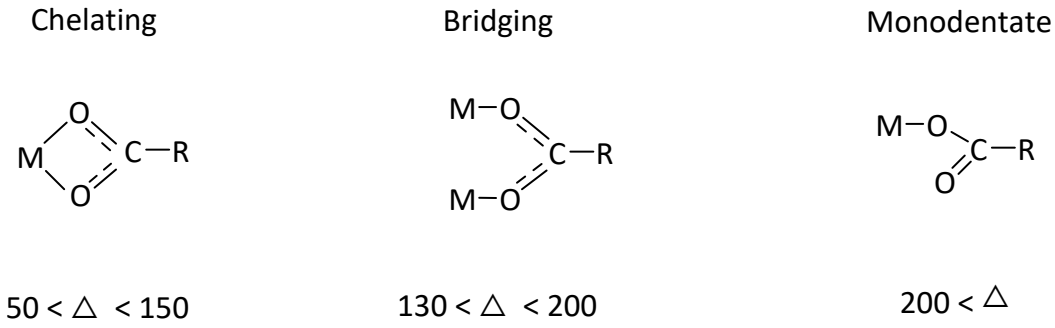

b

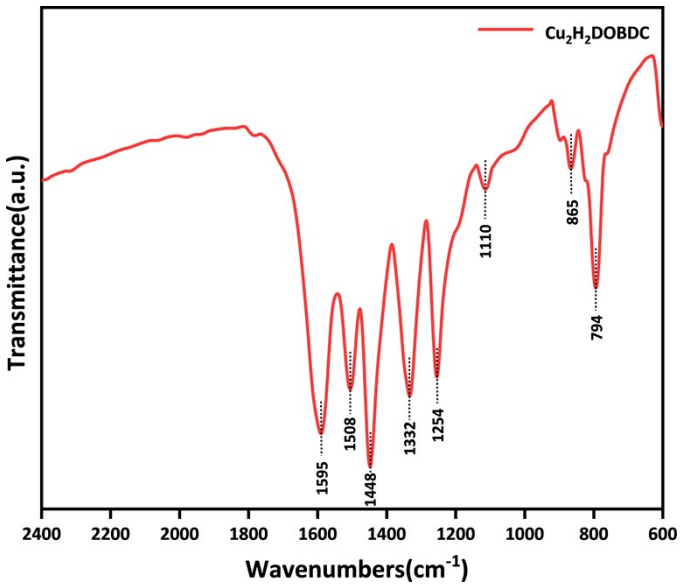

Figure S6. (a) Three coordination modes and corresponding Δ values for carboxylate ion and metal (M). (b) FTIR spectrum of Cu_2H_2DOBDC and assignment of typical bands.

Consistent with previous studies in the literature,[2-5] FTIR bands for Cu_2H_2DOBDC are observed at 1595, 1508, 1448, 1332, 1254, 1110, 865, and 794 cm^{-1}. The asymmetric stretch of the carboxylate group is present at 1595 cm^{-1}, while the symmetric stretch is observed at 1332 cm^{-1}. The other bands observed in Cu_2H_2DOBDC are as follows: 1508 cm^{-1} is assigned to the ring vibrations of phenyl groups, 1448 cm^{-1} corresponds to the in-plane OH deformation modes, 1254 cm^{-1} is attributed to the C-OH combination band of a carboxylic acid, 1110 cm^{-1} is assigned to the C-H in-plane bending modes, and the bands at 865 and 794 cm^{-1} coincide with the C-C ring out-of-plane bending modes.

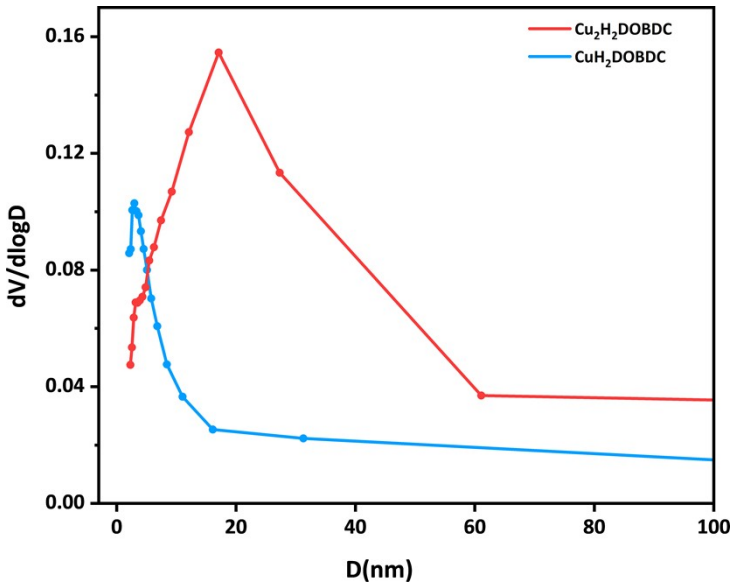

Figure S7. Pore size distributions of CuH_2DOBDC and Cu_2H_2DOBDC.

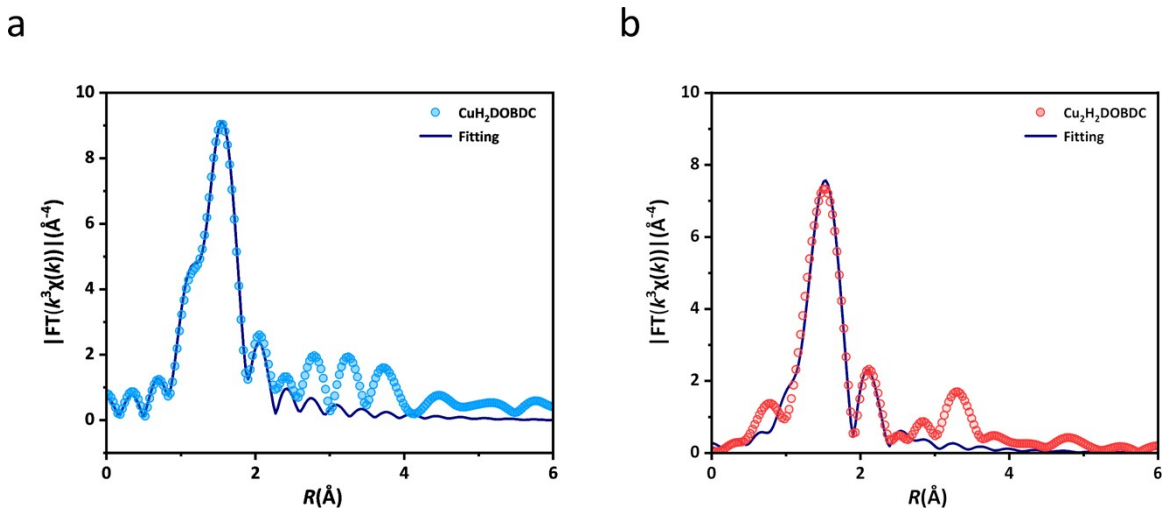

Figure S8. EXAFS fitting results of FT-EXAFX spectra at the Cu K-edge of (a) CuH_2DOBDC, (b) Cu_2H_2DOBDC at the R spaces.

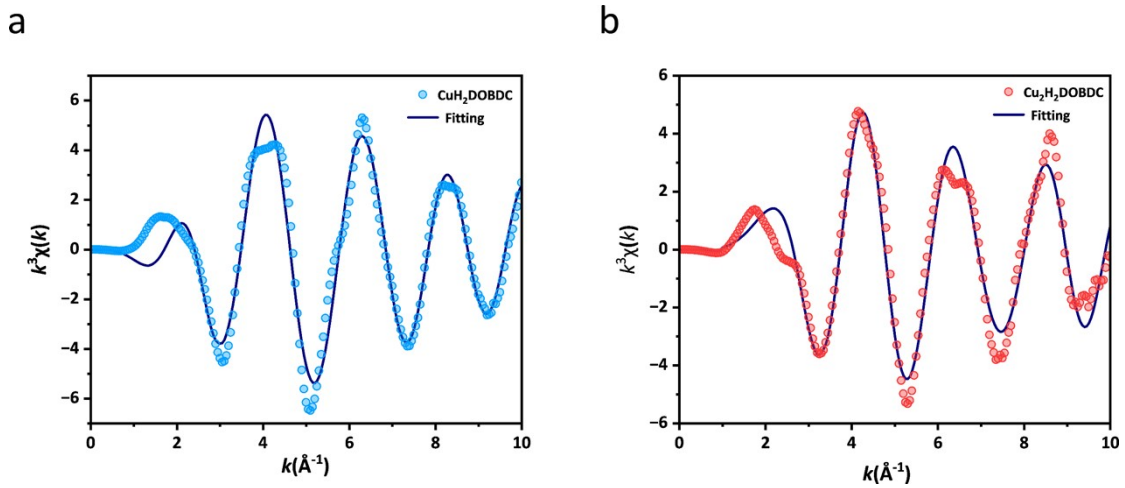

Figure S9. EXAFS fitting results of FT-EXAFX spectra at the Cu K-edge of (a) CuH_2DOBDC, (b) Cu_2H_2DOBDC at the K spaces.

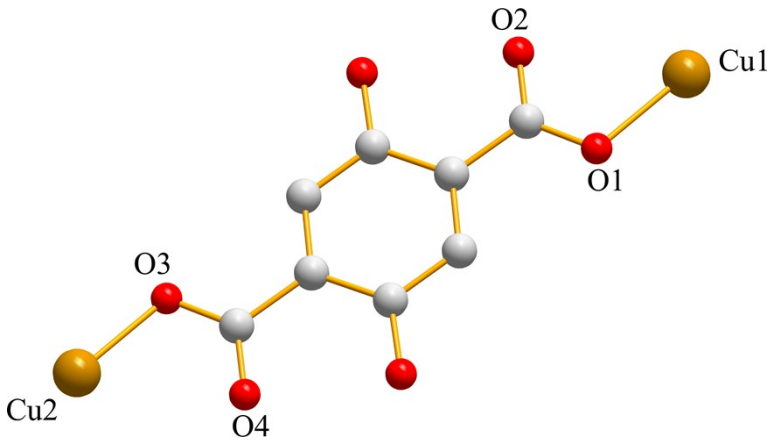

Figure S10. Speculation on the local structure of Cu_2H_2DOBDC.

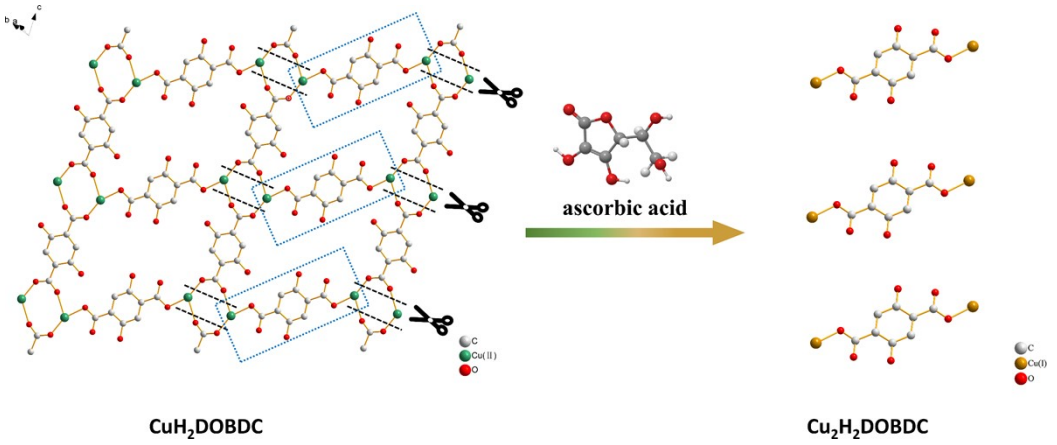

Figure S11. Possible formation process of Cu_2H_2DOBDC local structure.

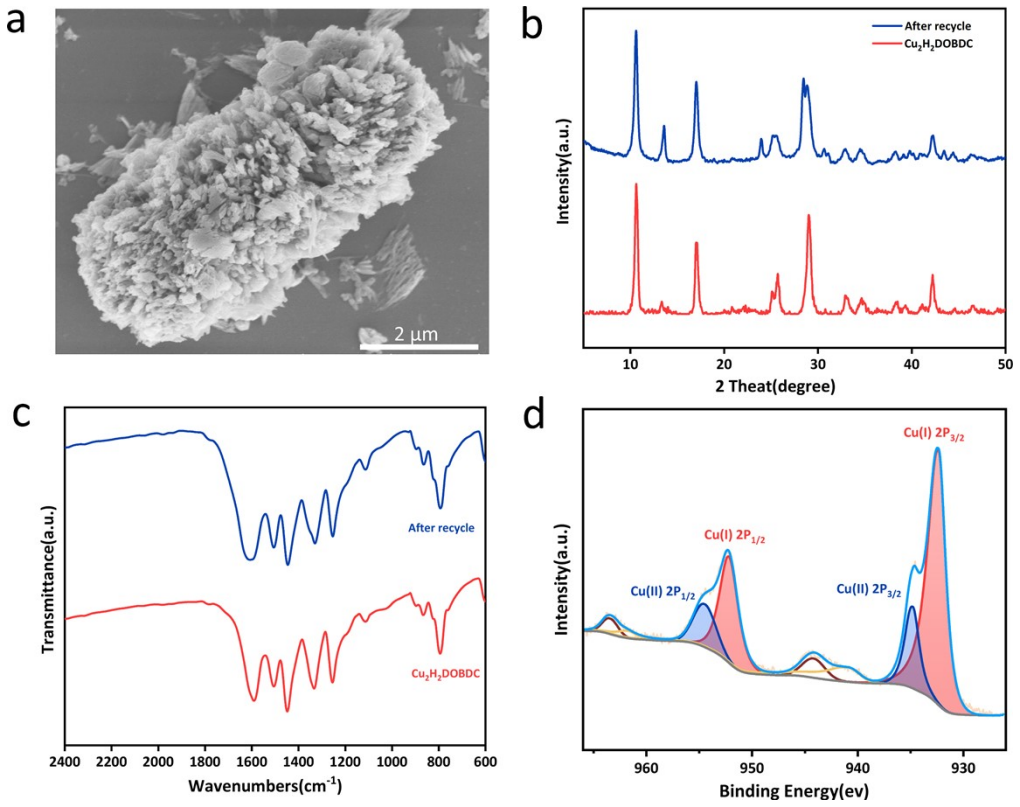

Figure S12. Cu_2H_2DOBDC after five cycles recycle. (a) SEM images. (b) XRD patterns. (c) FTIR spectra. (d) XPS spectra for Cu 2p.

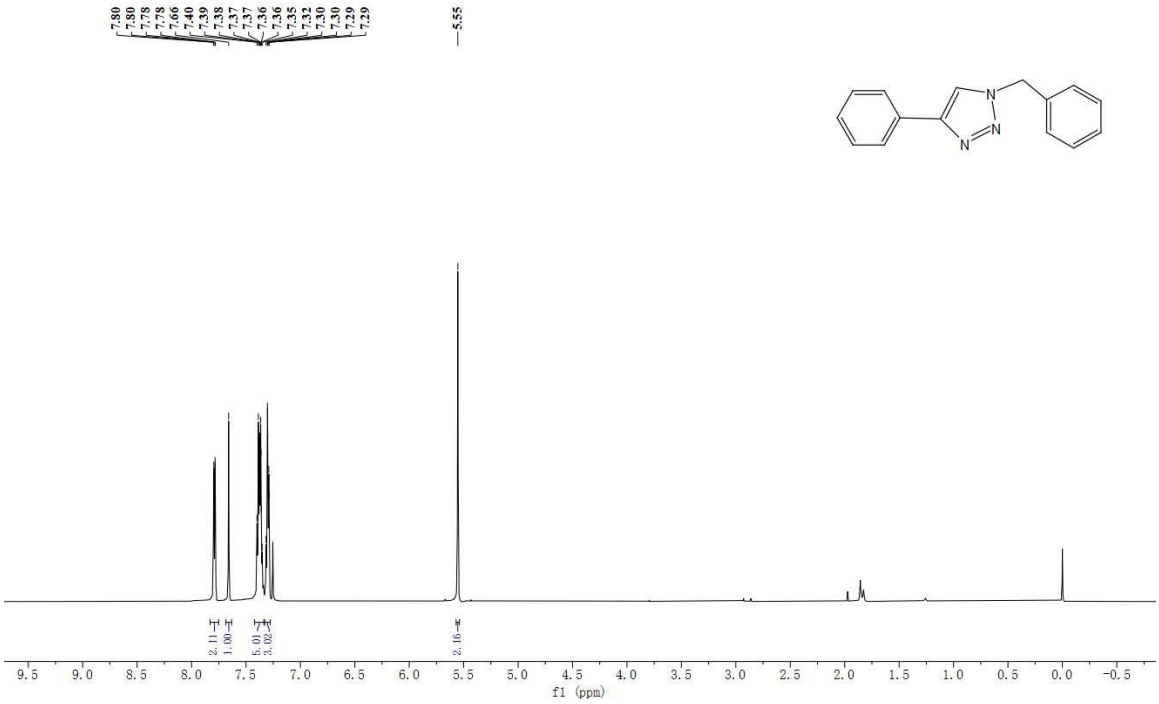

Figure S13. ^{1}H NMR (600 MHz, $CDCl_3$) for 1-benzyl-4-phenyl-1*H*-1,2,3-triazole: δ 7.83 - 7.75 (m, 2H), 7.66 (s, 1H), 7.42 - 7.34 (m, 5H), 7.33 - 7.28 (m, 3H), 5.55 (s, 2H).

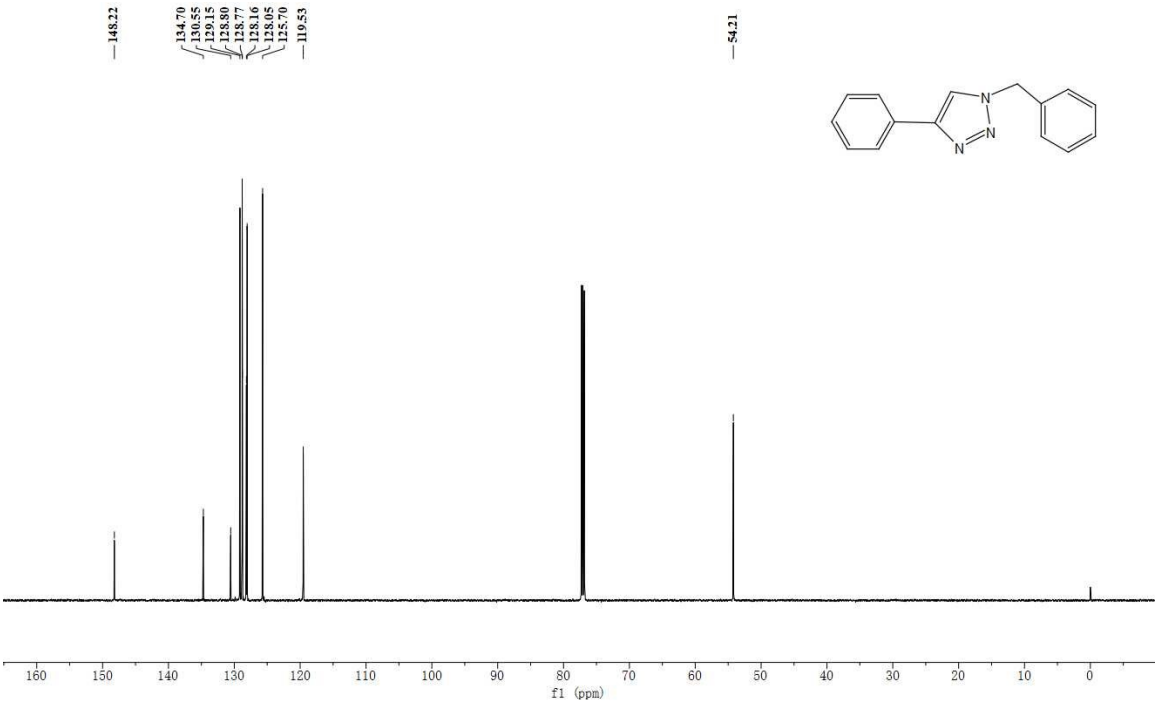

Figure S14. ^{13}C NMR (151 MHz, $CDCl_3$) for 1-benzyl-4-phenyl-1*H*-1,2,3-triazole: δ 148.22, 134.70, 130.55, 129.15, 128.80, 128.77, 128.16, 128.05, 125.70, 119.53, 54.21.

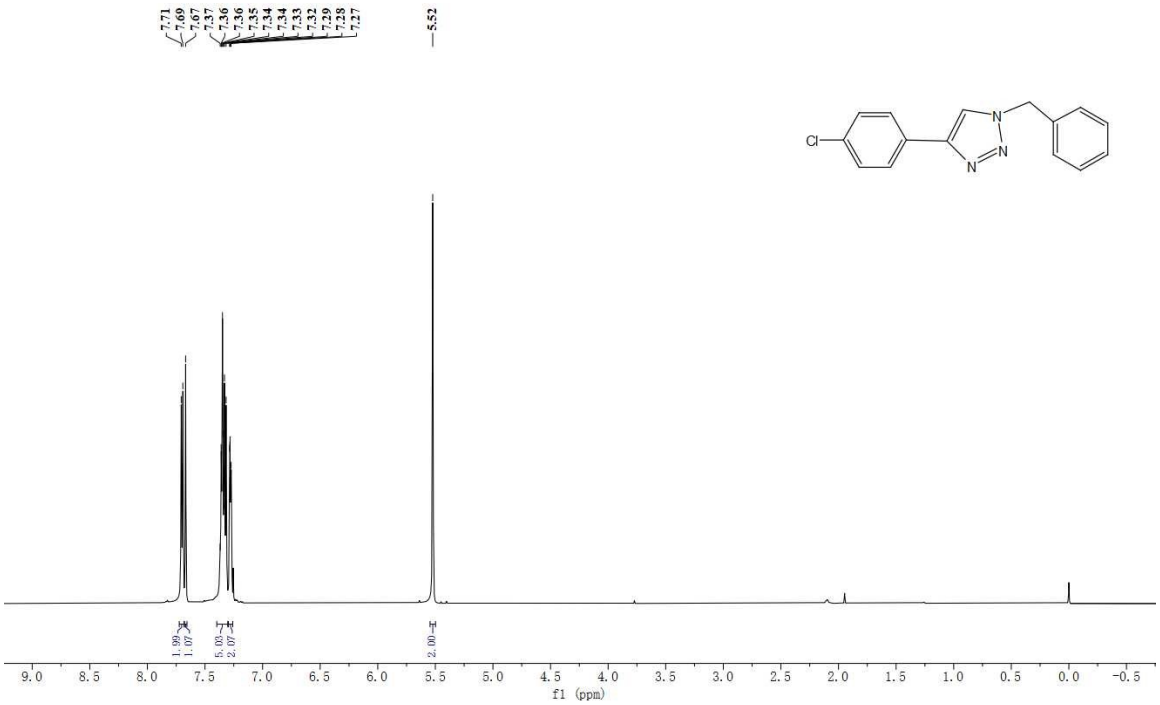

Figure S15. ^{1}H NMR (600 MHz, $CDCl_3$) for 1-benzyl-4-(4-chlorophenyl)-1H-1,2,3-triazole: δ 7.70(d, 2H), 7.67 (s, 1H), 7.40 - 7.30 (m, 5H), 7.30 - 7.26 (m, 2H), 5.52 (s, 2H).

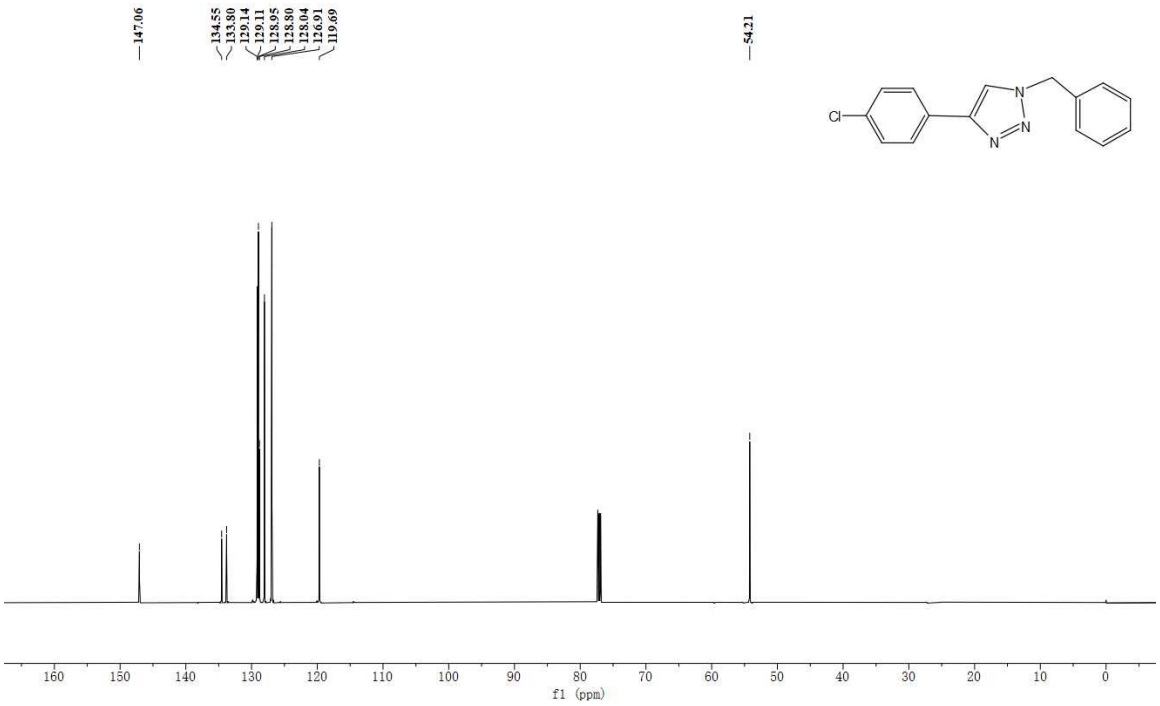

Figure S16. ^{13}C NMR (151 MHz, $CDCl_3$) for 1-benzyl-4-(4-chlorophenyl)-1*H*-1,2,3-triazole: δ 147.06, 134.55, 133.80, 129.14, 129.11, 128.95, 128.80, 128.04, 126.91, 119.69, 54.21.

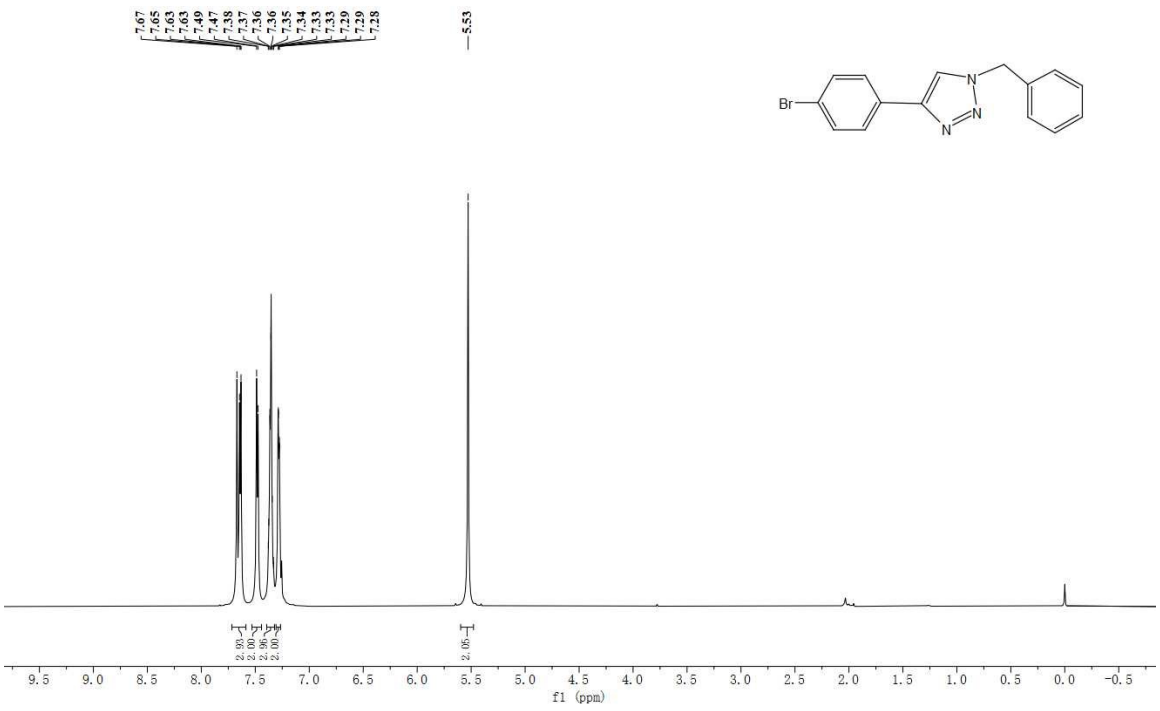

Figure S17. ^{1}H NMR (600 MHz, $CDCl_3$) for 1-benzyl-4-(4-bromophenyl)-1*H*-1,2,3-triazole: δ 7.67 - 7.63 (m, 3H), 7.48 (d, 2H), 7.38 - 7.33 (m, 3H), 7.29 - 7.28 (m, 2H), 5.53 (s, 2H).

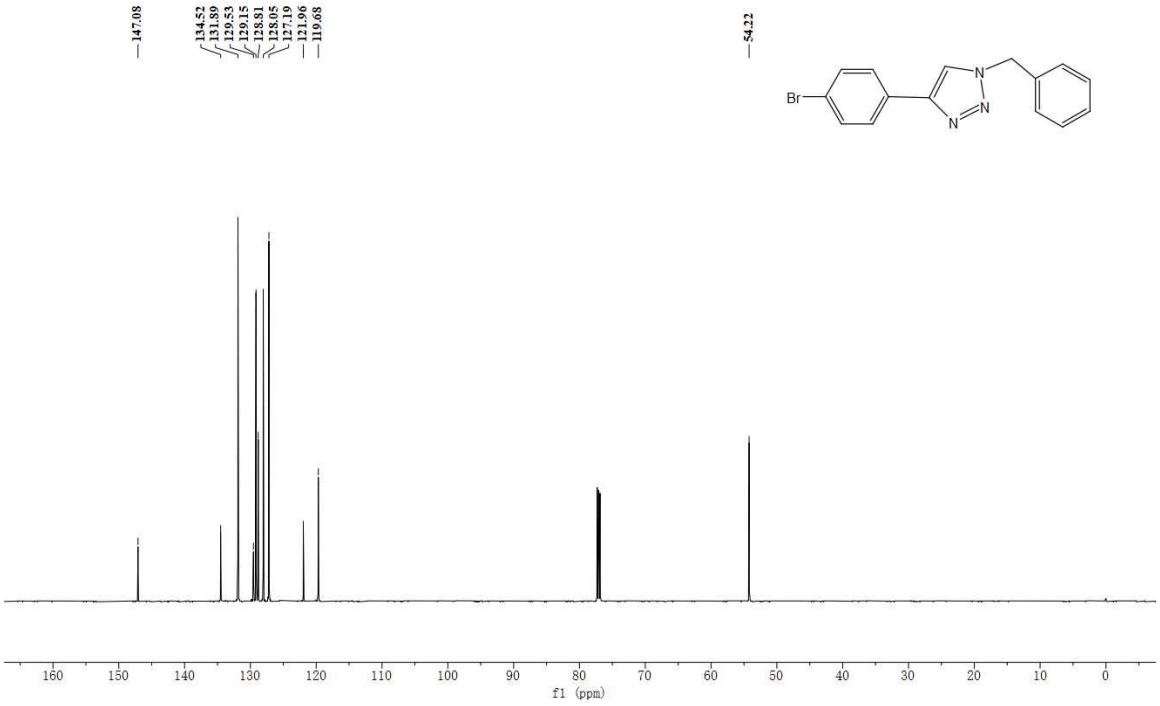

Figure S18. ^{13}C NMR (151 MHz, $CDCl_3$) for 1-benzyl-4-(4-bromophenyl)-1*H*-1,2,3-triazole: δ 147.08, 134.52, 131.89, 129.53, 129.15, 128.81, 128.05, 127.19, 121.96, 119.68, 54.22.

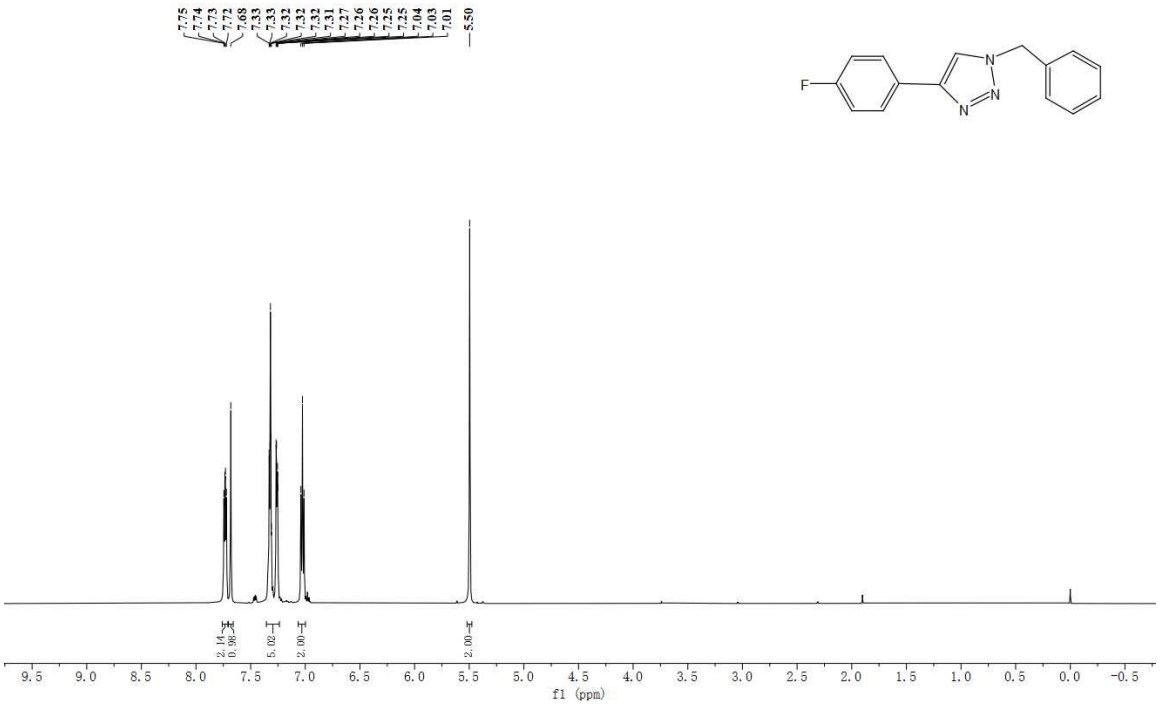

Figure S19. ^{1}H NMR (600 MHz, $CDCl_3$) for 1-benzyl-4-(4-fluorophenyl)-1*H*-1,2,3-triazole: δ 7.75 - 7.72 (m, 2H), 7.68 (s, 1H), 7.33 - 7.25 (m, 5H), 7.04 - 7.01 (m, 2H), 5.50 (s, 2H).

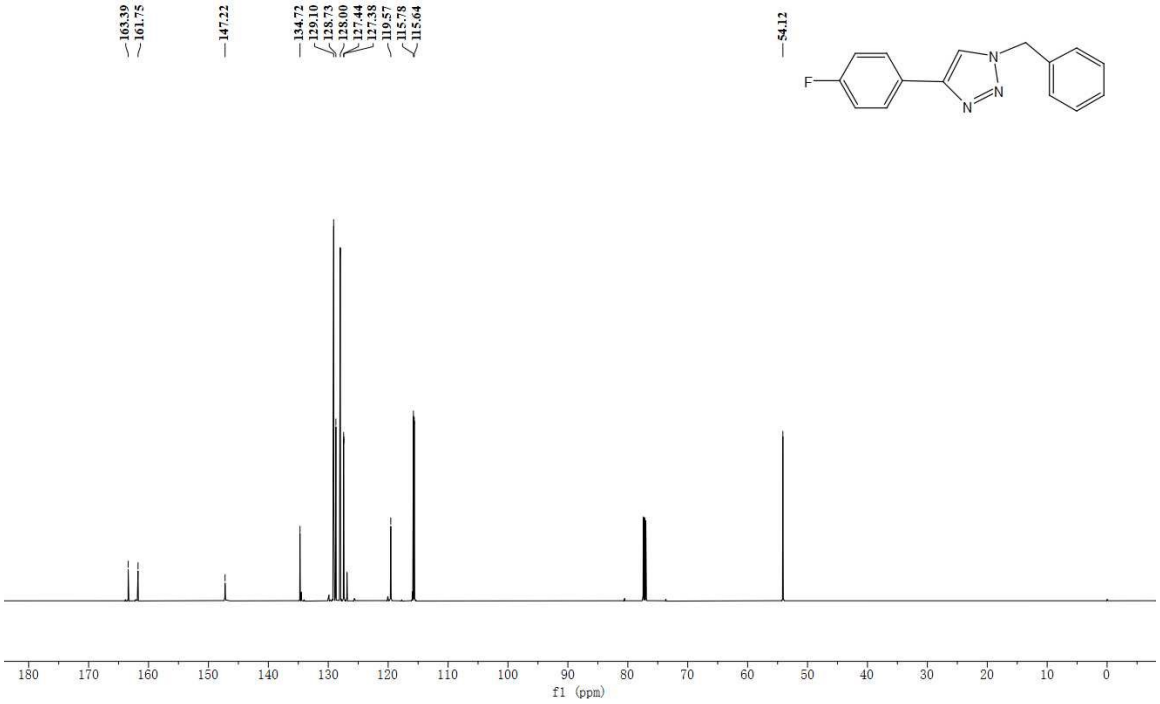

Figure S20. ^{13}C NMR (151 MHz, $CDCl_3$) for 1-benzyl-4-(4-fluorophenyl)-1*H*-1,2,3-triazole: δ 163.39, 161.75, 147.22, 134.72, 129.10, 128.73, 128.00, 127.44, 127.38, 119.57, 115.78, 115.64, 54.12.

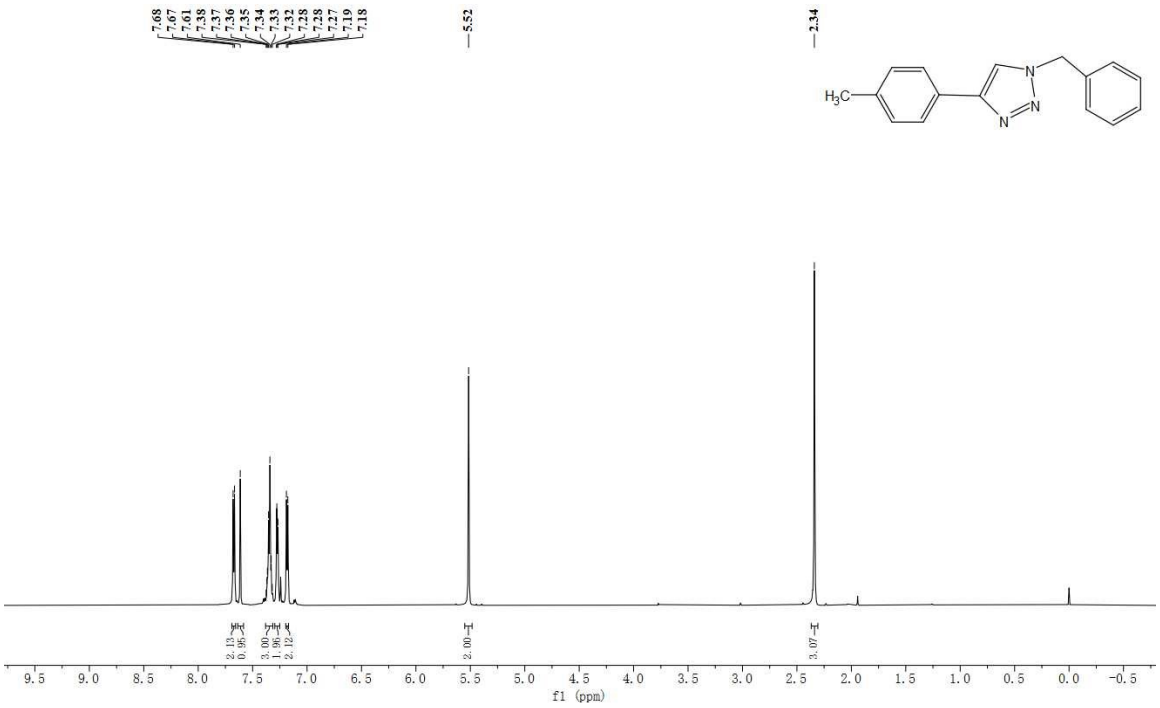

Figure S21. ^{1}H NMR (600 MHz, $CDCl_3$) for 1-benzyl-4-(p-tolyl)-1*H*-1,2,3-triazole: δ 7.67 (d, 2H), 7.61 (s, 1H), 7.38 - 7.32 (m, 3H), 7.28 - 7.27 (m, 2H), 7.18 (d, 2H), 5.52 (s, 2H), 2.34 (s, 3H).

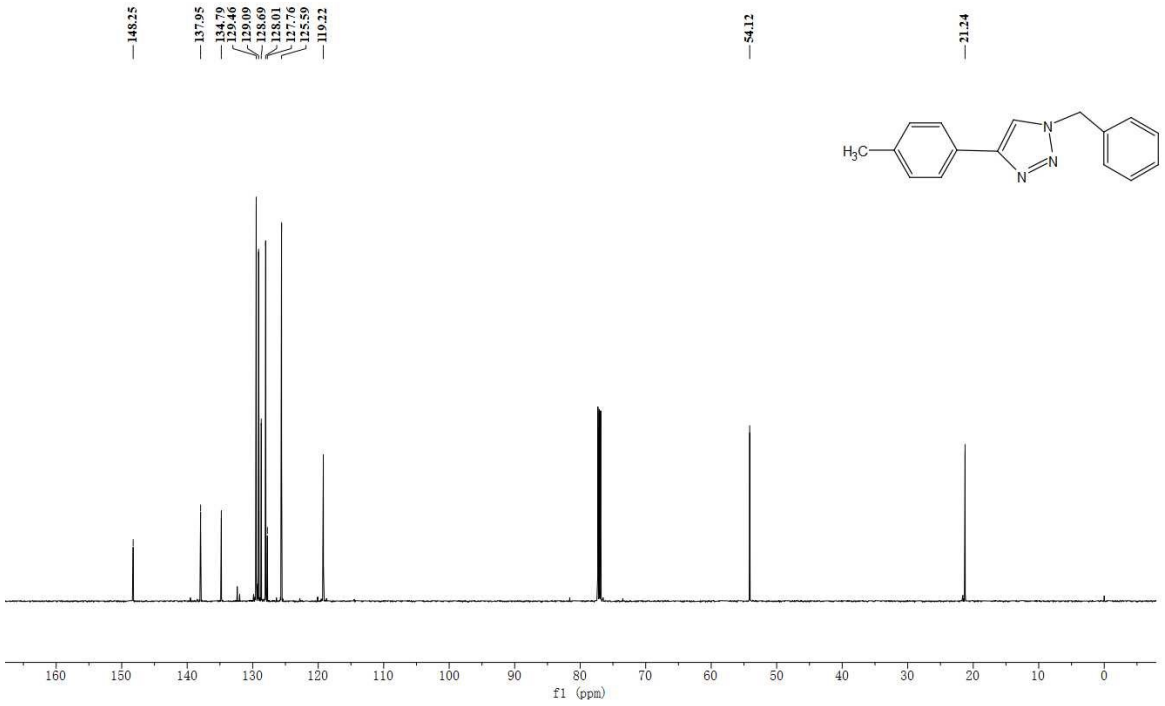

Figure S22. ^{13}C NMR (151 MHz, $CDCl_3$) for 1-benzyl-4-(p-tolyl)-1*H*-1,2,3-triazole: δ 148.25, 137.95, 134.79, 129.46, 129.09, 128.69, 128.01, 127.76, 125.59, 119.22, 54.12, 21.24.

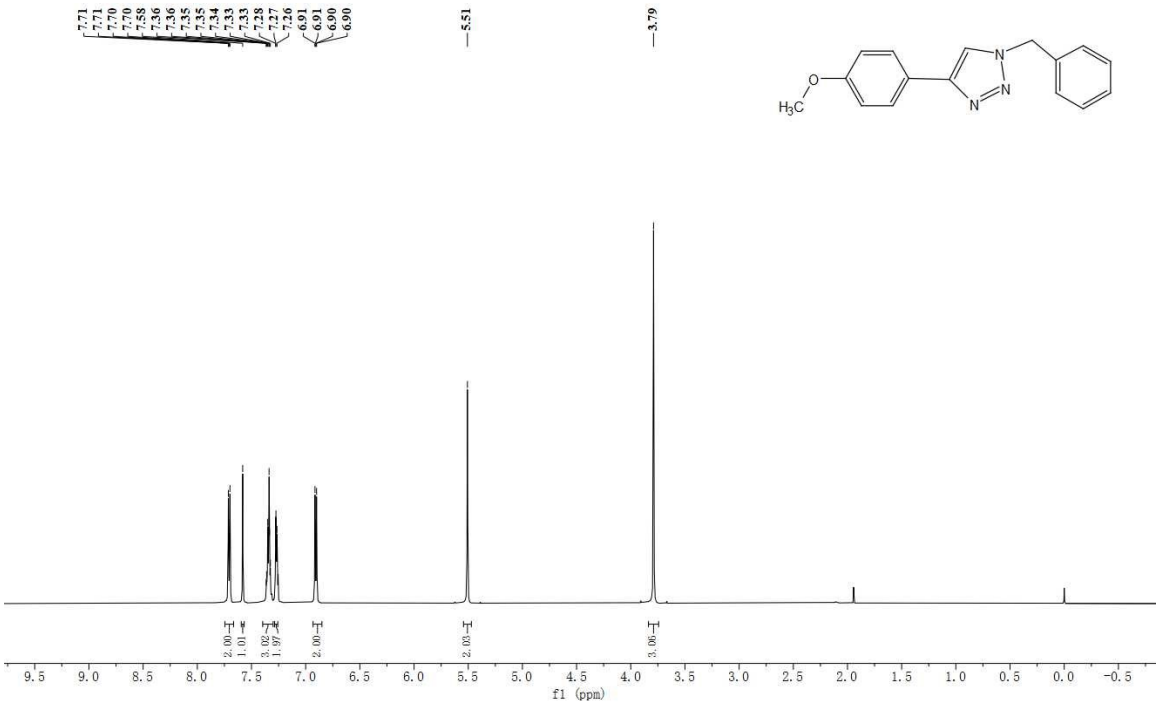

Figure S23. ^{1}H NMR (600 MHz, $CDCl_3$) for 1-benzyl-4-(4-methoxyphenyl)-1*H*-1,2,3-triazole: δ 7.74 - 7.66 (m, 2H), 7.58 (s, 1H), 7.36 - 7.33 (m, 3H), 7.29 - 7.26 (m, 2H), 6.93 - 6.85 (m, 2H), 5.51 (s, 2H), 3.79 (s, 3H).

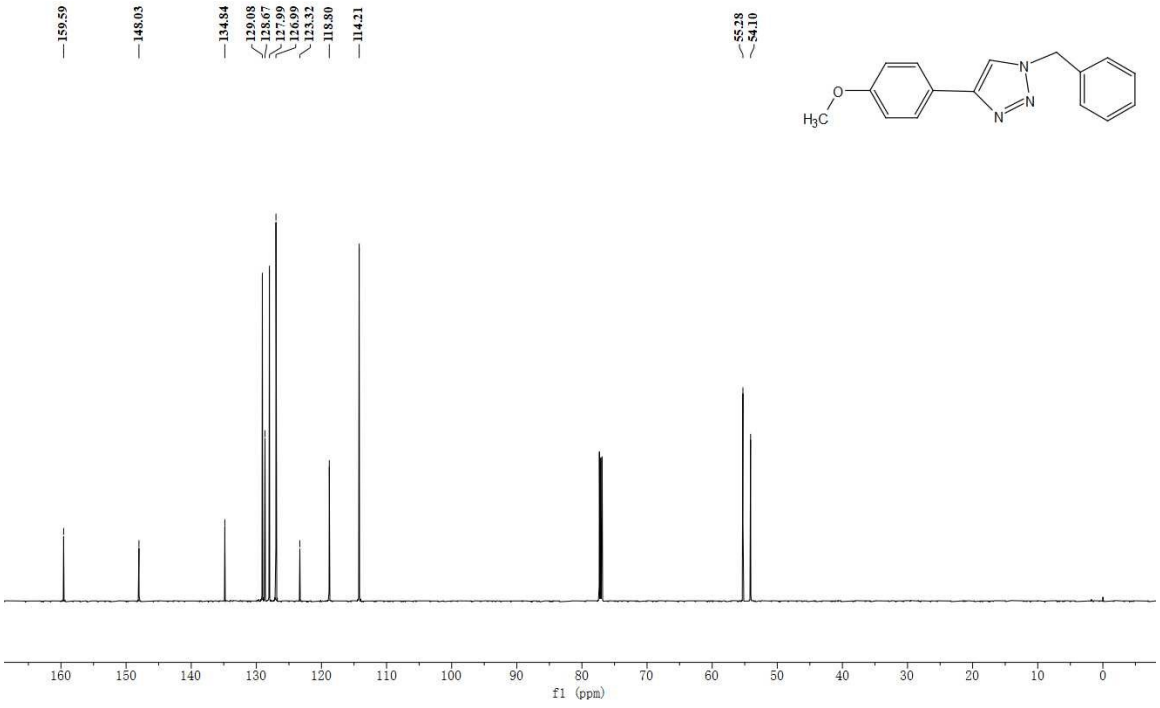

Figure S24. ^{13}C NMR (151 MHz, $CDCl_3$) for 1-benzyl-4-(4-methoxyphenyl)-1*H*-1,2,3-triazole: δ 159.59, 148.03, 134.84, 129.08, 128.67, 127.99, 126.99, 123.32, 118.80, 114.21, 55.28, 54.10.

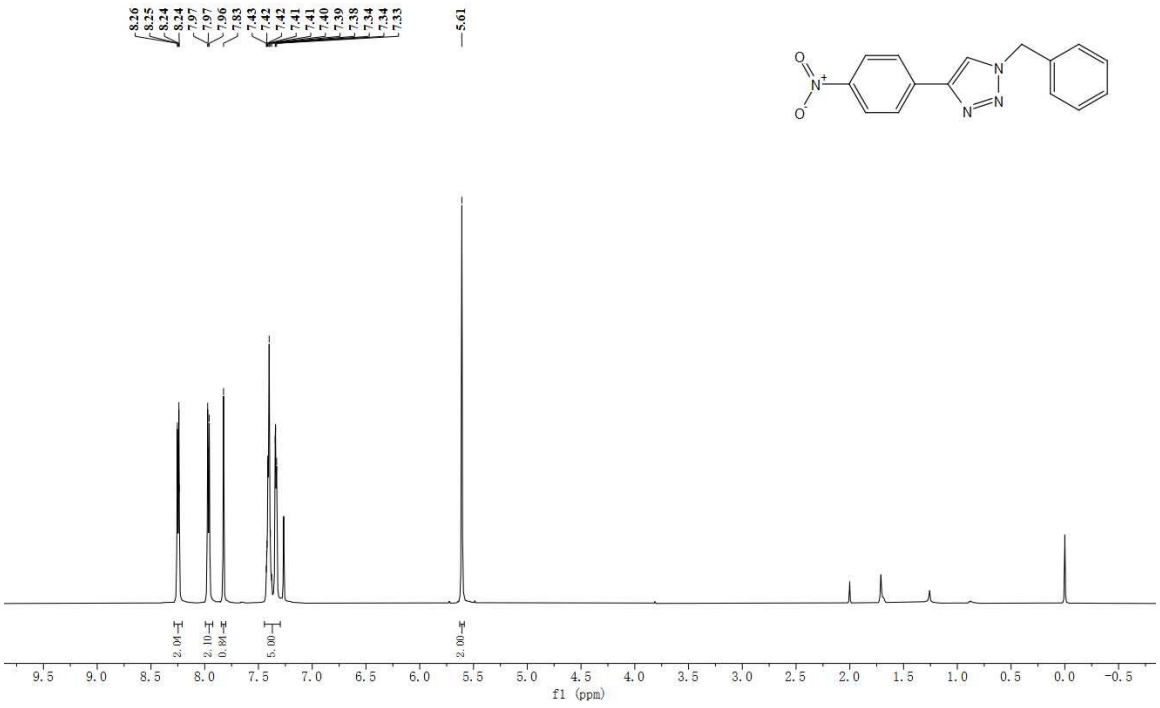

Figure S25. ^{1}H NMR (600 MHz, $CDCl_3$) for 1-benzyl-4-(4-nitrophenyl)-1H-1,2,3-triazole: δ 8.25 (d, 2H), 7.99 - 7.92 (m, 2H), 7.83 (s, 1H), 7.44 - 7.30 (m, 5H), 5.61 (s, 2H).

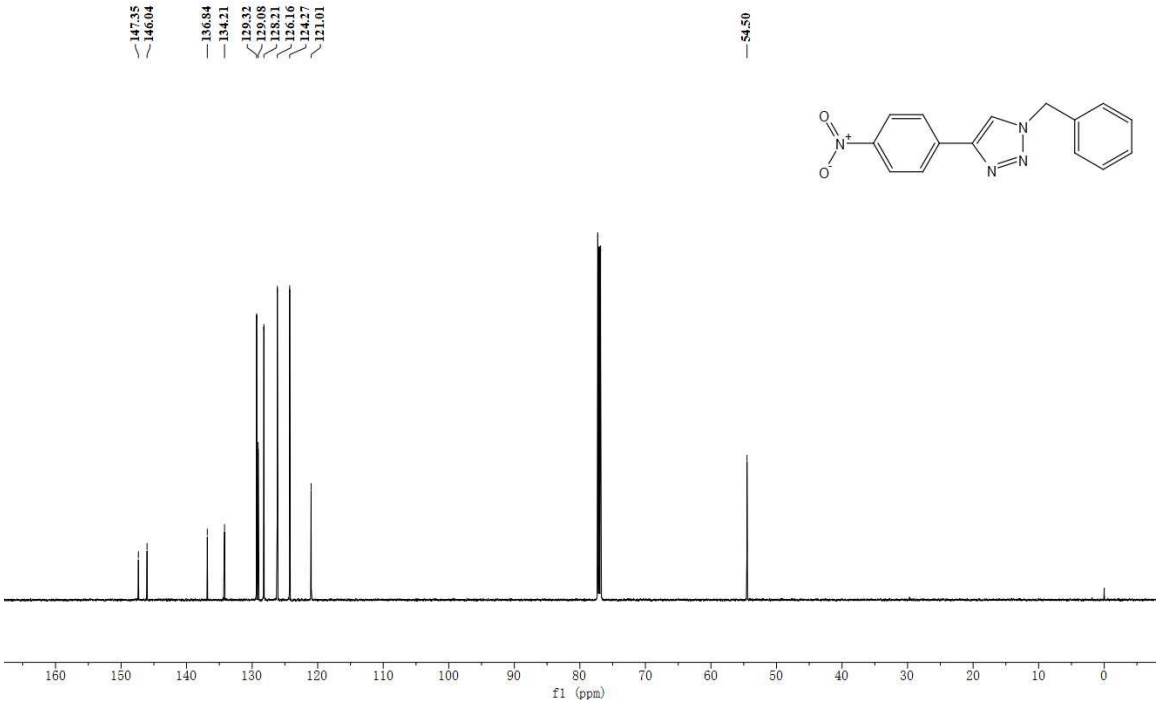

Figure S26. ^{13}C NMR (151 MHz, $CDCl_3$) for 1-benzyl-4-(4-nitrophenyl)-1H-1,2,3-triazole: δ 147.35, 146.04, 136.84, 134.21, 129.32, 129.08, 128.21, 126.16, 124.27, 121.01, 54.50.

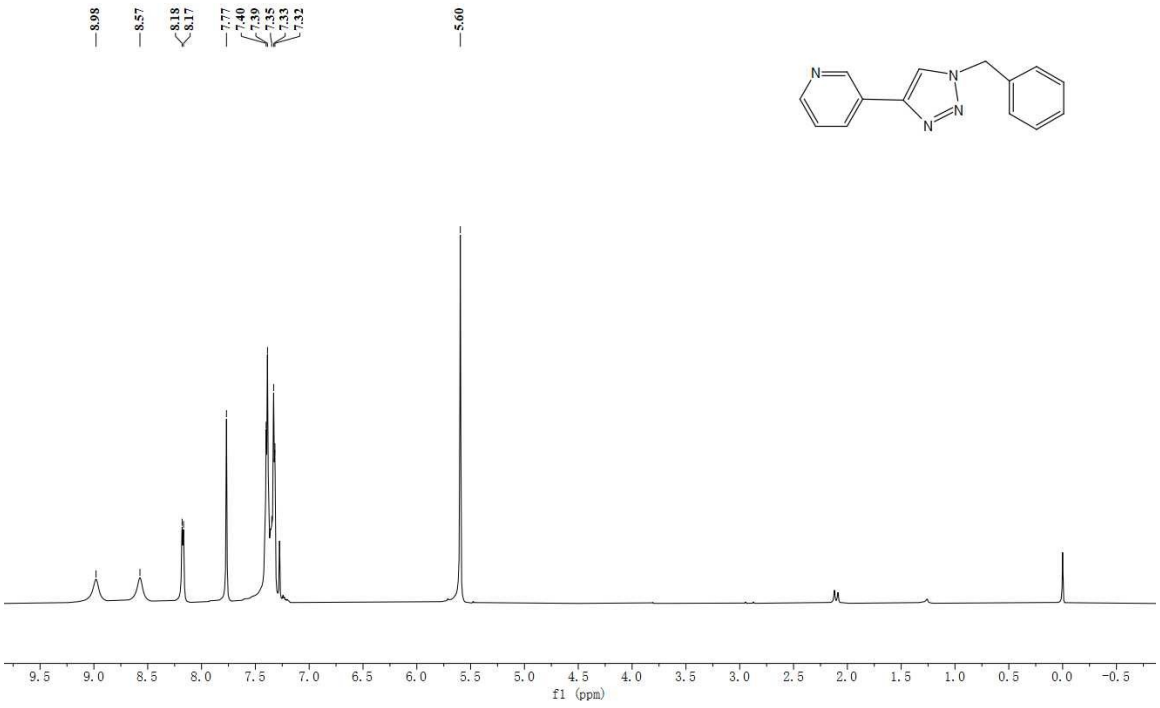

Figure S27. ^{1}H NMR (600 MHz, $CDCl_3$) for 3-(1-benzyl-1*H*-1,2,3-triazol-4-yl)pyridine: δ 8.98 (s, 1H), 8.57 (s, 1H), 8.17 (d, 1H), 7.77 (s, 1H), 7.43 - 7.30 (m, 6H), 5.60 (s, 2H).

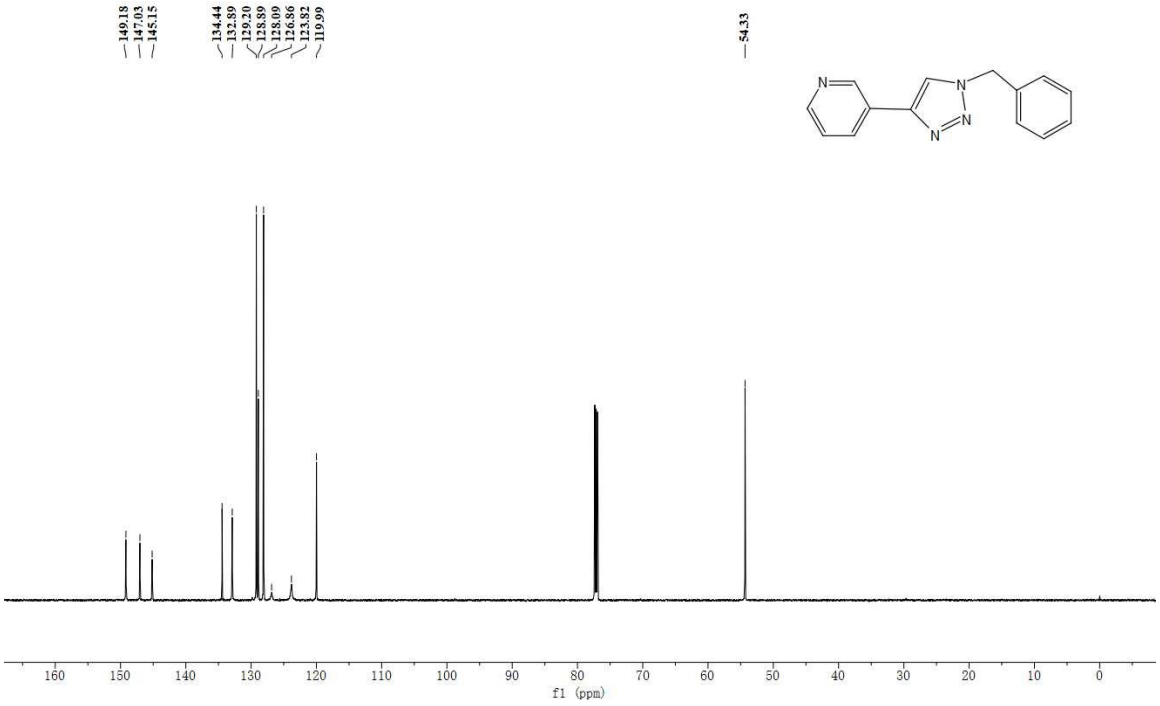

Figure S28. ^{13}C NMR (151 MHz, $CDCl_3$) for 3-(1-benzyl-1*H*-1,2,3-triazol-4-yl)pyridine: δ 149.18, 147.03, 145.15, 134.44, 132.89, 129.20, 128.89, 128.09, 126.86, 123.82, 119.99, 54.33.

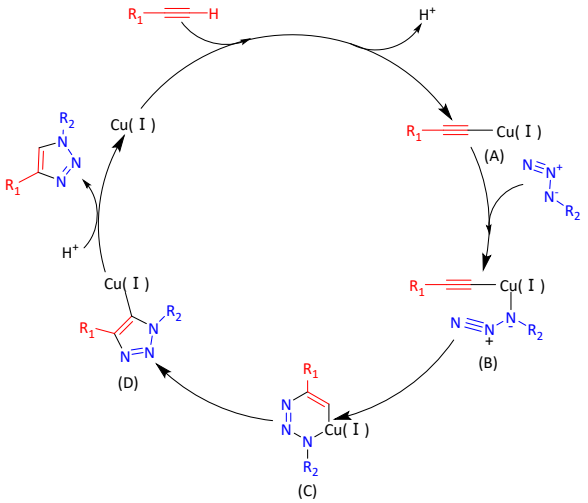

Figure S29. Proposed Catalytic Mechanism for the CuAAC Reaction with Cu_2H_2DOBDC as a catalyst**.**

Table S1. ICP results of CuH_2DOBDC and Cu_2H_2DOBDC

Sample	Cu%
CuH_2DOBDC	13.8
Cu_2H_2DOBDC	36.1

Table S2. EXAFS fitting parameters at the Cu K-edge of CuH_2DOBDC and Cu_2H_2DOBDC.

Sample	Path	*N*[a]	*R*(Å)[b]	σ² (Å²)[c]	ΔE_0(eV)[d]	*R* factor
CuH_2DOBDC	Cu-O	6.21 ± 0.69	1.96 ± 0.012	0.008 ± 0.001	0.43 ± 1.56	0.0036
Cu_2H_2DOBDC	Cu-O	4.01 ± 0.68	1.94 ± 0.015	0.006 ± 0.002	3.58 ± 2.04	0.0047

EXAFS fitting parameters at the Cu K-edge for various samples. (S_0^2 =1.0)

[a]*N* : coordination numbers; [b]*R* : bond distance; [c]σ^2 : Debye-Waller factors; [d]ΔE_0 : the inner potential correction. R factor: goodness of fit. S_0^2 was set to 1.0, according to the experimental EXAFS fit of Cu foil reference by fixing CN as the known crystallographic value;

δ: percentage.

Table S3 Optimization of the reaction conditions for the catalytic reactions of benzyl azide with phenylacetylene[a]

Entry	Catalyst	Amount (mg)	Temperature(°C)	Yield(%)[b]
1	Cu_2H_2DOBDC	10	RT	26
2	Cu_2H_2DOBDC	10	60	74
3	Cu_2H_2DOBDC	10	80	99
4	Cu_2H_2DOBDC	5	80	79
5	CuH_2DOBDC	10	80	39
6	No catalyst	0	80	19

[a]Reaction conditions: benzyl azide (1 mmol), phenylacetylene (2 mmol), amyl acetate (1 mmol), acetonitrile (4 ml) and reaction time (2.5 h). [b]Isolated yields were calculated by GC and the amyl acetate was employed as the internal standard.

Table S4 Summary of the previously reported Cu-based catalysts and the Cu_2H_2DOBDC catalyst for the Azide-Alkyne "Click" Reaction.

Catalyst	Reaction Conditions	Yield	Reference
Cu_2H_2DOBDC	80℃, 2.5 h	99%	This Work
$[Cu^{I}_4(SiW_{12}O_{40})(L)]\cdot 6H_2O\cdot 2DMF$	80℃, 24 h	99%	6
DE-CuBTC (CuICuII-BTC)	70℃, 6 h	100%	7
$Cu_3(Br)_3(L)$	70℃, 8 h	>99%	8
Cu_1/NC-800	RT, 12 h	>99%	9
$[Cu_4Cl_4L]\cdot CH_3OH\cdot 1.5H_2O$	60℃, 8 h	99%	10
$Cu_4(SiW_{12}O_{40})(L)_2(DMF)_2]\cdot 2EtOH\cdot DMF$	80℃, 12 h	99%	11
saCu-2@mpgC_3N_4	130℃, 0.5 h	45%	12
Cu(I)-containing MONPs	50℃, 24 h	>99%	13
Cu(PTZ)(NSA) $0.5\cdot H_2O$	50℃, 2.5 h	94%	14
$[2Cu(L)(A)\cdot 3H_2O]_n$	80℃, 24 h	>99%	15

References

1 L. Valenzano, B. Civalleri, S. Chavan, S. Bordiga, M. H. Nilsen, S. Jakobsen, K. P. Lillerud and C. Lamberti, Disclosing the Complex Structure of UiO-66 Metal Organic Framework: A Synergic Combination of Experiment and Theory, *Chem. Mater.,* 2011, **23**, 1700-1718.

2 X. Zhou, J. Dong, Y. Zhu, L. Liu, Y. Jiao, H. Li, Y. Han, K. Davey, Q. Xu, Y. Zheng and S. Z. Qiao, Molecular Scalpel to Chemically Cleave Metal-Organic Frameworks for Induced Phase Transition, *J. Am. Chem. Soc.,* 2021, **143**, 6681-6690.

3 L. Shao, F. Q. Fan, X. Y. Dai, H. X. Fu, W. Z. Li, W. Qi, F. B. Meng and Y. Fu, Pseudomorphic Replacement in the Transformation between Metal-Organic Frameworks toward Three-Dimensional Hierarchical Nanostructures, *Chem. Mater.,* 2022, **34**, 5356-5365.

4 C. Huang, J. Dong, W. Sun, Z. Xue, J. Ma, L. Zheng, C. Liu, X. Li, K. Zhou, X. Qiao, Q. Song, W. Ma, L. Zhang, Z. Lin and T. Wang, Coordination mode engineering in stacked-nanosheet metal-organic frameworks to enhance catalytic reactivity and structural robustness, *Nat. Commun.,* 2019, **10**, 2779.

5 S. Shetty and R. A. van Santen, CO as an IR probe molecule for characterization of copper ions in a basolite C300 MOF sample, *Phys. Chem. Chem. Phys.,* 2010, **12**, 6330-6332.

6 B.-B. Lu, J. Yang, G.-B. Che, W.-Y. Pei and J.-F. Ma, Highly Stable Copper(I)-Based Metal-Organic Framework Assembled with Resorcin[4]arene and Polyoxometalate for Efficient Heterogeneous Catalysis of Azide-Alkyne "Click" Reaction, *ACS Appl. Mater. Interfaces,* 2018, **10**, 2628-2636.

7 Z. Fan, Z. Wang, M. Cokoja and R. A. Fischer, Defect engineering: an effective tool for enhancing the catalytic performance of copper-MOFs for the click reaction and the A^3 coupling, *Catal. Sci. Technol.,* 2021, **11**, 2396-2402.

8 J. F. Li, P. Du, Y. Y. Liu, G. H. Xu and J. F. Ma, Three thiacalix[4]arene-based Cu(I) coordination polymers: catalytic activities for azide-alkyne cycloaddition reactions and luminescence properties, *Dalton Trans.,* 2020, **49**, 3715-3722.

9 P. Ren, Q. Li, T. Song, Z. Wang, K. Motokura and Y. Yang, Highly Efficient and Stable Atomically Dispersed Cu Catalyst for Azide-Alkyne Cycloaddition Reaction, *ChemCatChem,* 2021, **13**, 3960-3966.

10 X. X. Wang, J. Yang, X. Xu and J. F. Ma, Highly Stable Copper(I)-Thiacalix[4]arene-Based Frameworks for Highly Efficient Catalysis of Click Reactions in Water, *Chemistry,* 2019, **25**, 16660-16667.

11 M. Y. Yu, T. T. Guo, X. C. Shi, J. Yang, X. Xu, J. F. Ma and Z. T. Yu, Polyoxometalate-Bridged Cu(I)- and Ag(I)-Thiacalix[4]arene Dimers for Heterogeneous Catalytic Oxidative Desulfurization and Azide-Alkyne "Click" Reaction, *Inorg. Chem.,* 2019, **58**, 11010-11019.

12 G. Vilé, G. Di Liberto, S. Tosoni, A. Sivo, V. Ruta, M. Nachtegaal, A. H. Clark, S. Agnoli, Y. Zou, A. Savateev, M. Antonietti and G. Pacchioni, Azide-Alkyne Click Chemistry over a Heterogeneous Copper-Based Single-Atom Catalyst, *ACS Catal.,* 2022, **12**, 2947-2958.

13 Y. Bai, X. Feng, H. Xing, Y. Xu, B. K. Kim, N. Baig, T. Zhou, A. A. Gewirth, Y. Lu, E. Oldfield and S. C. Zimmerman, A Highly Efficient Single-Chain Metal-Organic Nanoparticle Catalyst for Alkyne-Azide "Click" Reactions in Water and in Cells, *J. Am. Chem. Soc.,* 2016, **138**, 11077-11080.

14 P. Li, S. Regati, H. Huang, H. D. Arman, J. C. G. Zhao and B. Chen, A metal-organic framework as a highly efficient and reusable catalyst for the solvent-free 1,3-dipolar cycloaddition of organic azides to alkynes, *Inorg. Chem. Front.,* 2015, **2**, 42-46.

15 K. Huang, Q. Li, X.-Y. Zhang, D.-B. Qin and B. Zhao, Copper-Cluster-Based MOF as a Heterogeneous Catalyst for CO_2 Chemical Fixation and Azide-Alkyne Cycloaddition, *Cryst. Growth Des.,* 2022, **22**, 6531-6538.